

Supporting Information for the manuscript

From pink to blue and back to pink again: changing the Co(II) ligation in a two-dimensional coordination network upon desolvation

D. Chisca,^a L. Croitor,^a E. B. Coropceanu,^b O. Petuhov,^b S. G. Baca,^a K. Krämer,^c S.-X. Liu,^c S. Decurtins,^c H. J. Rivera-Jacquez,^d A. E. Masunov,^{d,e} M. S. Fonari^{a*}

^a Institute of Applied Physics Academy of Sciences of R. Moldova, Academy str., 5 MD2028, Chisinau, Moldova; Tel.: + 373 22 738154; fax:+ 373 22 725887,

E-mail: fonari.xray@phys.asm.md;

^b Institute of Chemistry Academy of Sciences of R. Moldova, Academy str., 3 MD2028, Chisinau, Moldova;

^c Department of Chemistry and Biochemistry, University of Bern, Freiestrasse 3, 3012 Bern, Switzerland;

^d NanoScience Technology Center, 12424 Research Parkway Suite 400 Orlando, FL 32826 and Department of Chemistry, Department of Physics, and Florida Solar Energy Center, University of Central Florida, Orlando, Florida 32826, United States.

^e Department of Condensed Matter Physics, National Research Nuclear University MEPhI, Kashirskoye shosse 31, Moscow, 115409, Russia.

EXPERIMENTAL SECTION

Materials and general methods

All reagents and solvents were obtained from commercial sources and were used without further purification. Elemental analysis was performed on an Elementar Analysensysteme GmbH Vario El III elemental analyzer. The IR spectrum for **1** was recorded in a FT IR Spectrum-100 Perkin Elmer spectrometer in the range of 400 – 4000 cm⁻¹. The thermogravimetric analysis (TGA) was carried out with a Derivatograph Q-1500 thermal analyzer in an air flow at a heating rate of 5 °C/min in the temperature range of 25–1000 °C. The nitrogen adsorption-desorption isotherm has been measured using an Autosorb-1MP device. Magnetic susceptibility data were recorded using a Quantum design MPMS-5XL SQUID magnetometer in the temperature range 1.9 – 300 K and at a field of 1 kG. Experimental data were corrected for sample holder and diamagnetic contributions ($-0.45 \times \text{molecular weight} \times 10^{-6} \text{ cm}^3 \text{ mol}^{-1}$). The X-ray powder diffraction data for samples **1**, **dry_1**, and **dry_1s** were collected at room temperature on a DRON-UM, 30/30 kW/mA, 2×10^2 imp/sec, diffractometer using FeK α (av) radiation ($\lambda = 1.93604 \text{ \AA}$).

Single crystal X-ray crystallography

The crystallographic data for **1**, **dry_1**, and **dry_1s** were collected at a room temperature on a „Xcalibur Oxford Diffraction” diffractometer equipped with a CCD area detector and a graphite monochromator utilizing MoK α radiation, and were also recollected for **1** at 100 K on a 'SuperNova, Single source at offset, Eos', diffractometer equipped with a CCD area detector and a graphite monochromator utilizing MoK α radiation. Final unit cell dimensions were obtained and refined on an entire data set. All calculations to solve the structures and to refine the proposed models were carried out with the programs SHELXS-2014 and SHELXL-2014.¹ The structures **1** and **dry_1** were solved by direct methods and refined by full-matrix least-squares methods on F^2 by using the SHELXL-2014 program package.

Compound **1** is stable in ambient conditions for a long time that allowed recollected the single crystal X-ray data for this sample at 100 K. The data recollected for **1** at LT did not principally

change the disordering model while only revealing the explainable decrease of the unit cell volume and somewhat altered occupation factors for the disordered species in comparison with the RT data. In spite of the repeated attempts to run measurements at 173K and 253K (about 30 minutes each) for several crystals of **dry_1** even the best of them scatters only to about 1.9 Angstrom resolution. The forced unit is reasonably close to that one provided for the RT data. For consistency the discussion in the main body of the text refers to the RT experiments for all three compounds, **1**, **dry_1**, and **dry_1s** under discussion.

For **dry_1**, the data collection was carried out for the crystal subjected to the thermal stress that explains the significant deterioration of the crystal quality. The X-ray data were collected from a twin-crystal, and the structural model was found using the twin matrix and the HKLF5 procedure. For **dry_1s** obtained by **dry_1** soaking in methanol solution, only unit cell dimensions could be determined due to the further deterioration of the crystal quality. The Figures were produced using MERCURY and PLATON programs.^{2,3} The solvent accessible voids (SAVs) were calculated using PLATON.³ CCDC 1416671-1416672 contain the supplementary crystallographic data for **1** and **dry_1** at room temperature, and CCDC 1430303 contains the supplementary crystallographic data for **1** at 100 K. These data can be obtained free of charge from The Cambridge Crystallographic Data Centre via www.ccdc.cam.ac.uk/data_request/cif.

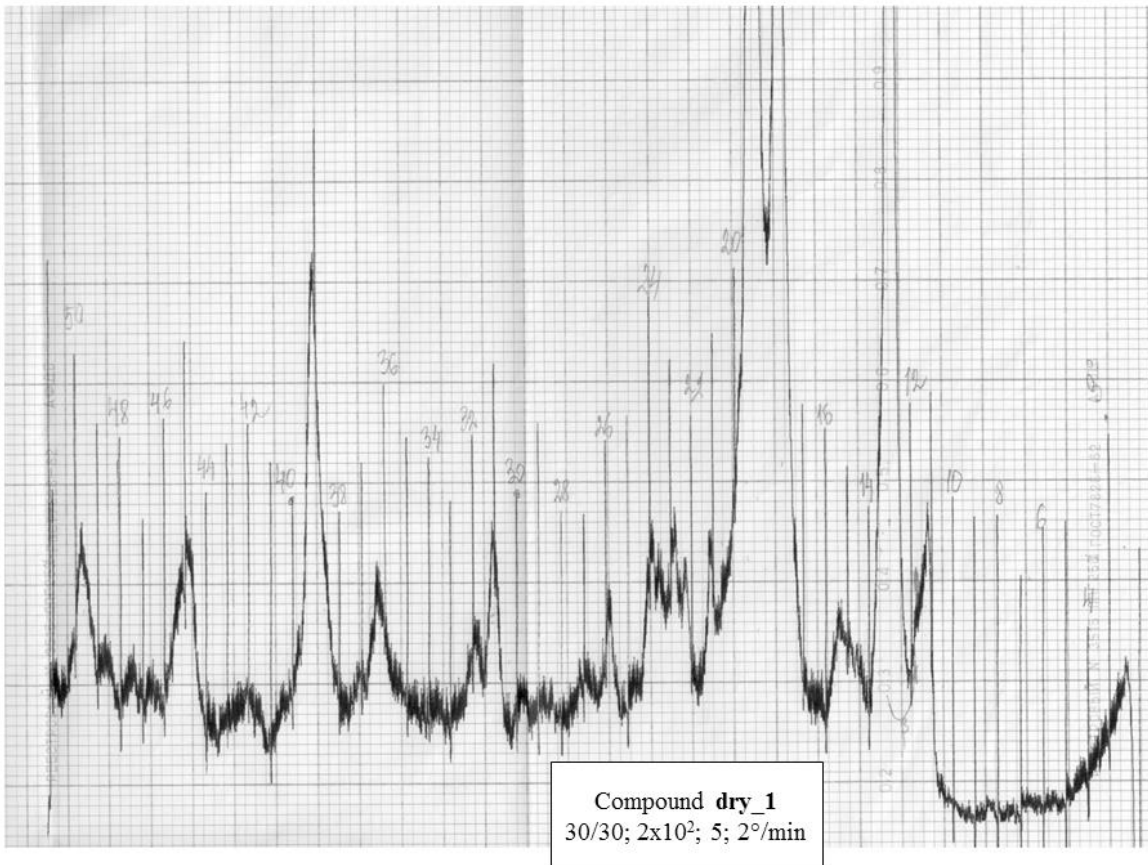
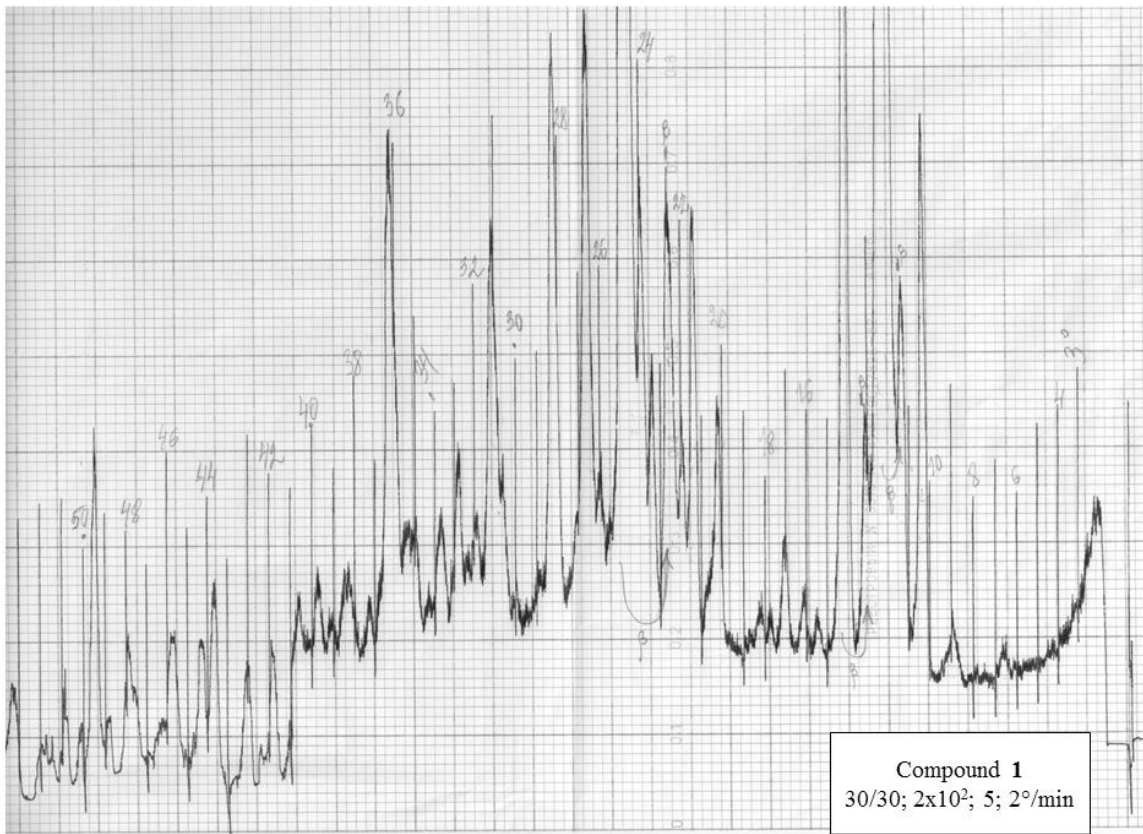
The X-ray powder diffraction patterns for **1**, **dry_1**, and **dry_1s** confirm their crystallinity, crystal purity of **1**, the presence of domains of **1** in bulk **dry_1** form as the minor impurity phase, and confirm conversion of **dry_1** to the new resolved form, **dry_1s** (Fig. 1S).

Synthesis and crystal data for 1: Co(CH₃COO)₂·4H₂O (0.025 g, 0.1 mmol) and thionicotinamide (0.028 g, 0.2 mmol) were dissolved in a mixture of CH₃OH:dmf:H₂O (6:3:2 ml) and stirred to form a tan solution. Then, H₂bdc (0.016 g, 1 mmol) was added and the solution was stirred for 30 min at 50 °C. Pink crystals precipitated upon cooling were filtered, washed with methanol and dmf and air dried. Yield, 58% (0.028 g). Elemental analysis for **1**, C₃₇H₄₇Co₂N₇O₁₄S₂, MW=995.80. Found, C 44.62, H 4.80, N 9.89. Calcd, C 44.58; H 4.72, N 9.84. IR (cm⁻¹): 3314 (s), 3204 (s), 1655 (m), 1377 (w), 1611 (m), 1600 (m), 1549 (v.s), 1500 (m), 1299 (v.s), 1152 (v.s), 1191 (s), 801 (w), 749 (w), 702 (w), 659 (w).

Crystal data for **1** (295 K): triclinic, space group *P*-1, *a* = 10.6132(5) Å, *b* = 13.4256(7) Å, *c* = 17.8366(12) Å; α = 78.860(5)°, β = 76.420(5)°, γ = 72.302(4)°; *V* = 2333.1(2) Å³; *Z* = 2; *D*_c = 1.417 g·cm⁻³; *F*(000) = 1032; μ = 0.868 mm⁻¹; *R*₁ = 0.0623, *wR*₂ = 0.1531 for 6842 independent reflections with *I* > 2σ(*I*); *R*₁ = 0.0796, *wR*₂ = 0.1623 for all 8623 independent reflections.

Crystal data for **1** (100 K) : triclinic, space group *P*-1, *a* = 10.5028(2) Å, *b* = 13.3758(3) Å, *c* = 17.9703(3) Å; α = 78.0998(15)°, β = 75.4371(16)°, γ = 71.7708(18)°; *V* = 2298.34(8) Å³; *Z* = 2; *D*_c = 1.439 g·cm⁻³; *F*(000) = 1032; μ = 0.882 mm⁻¹; *R*₁ = 0.0361, *wR*₂ = 0.0942 for 8403 independent reflections with *I* > 2σ(*I*); *R*₁ = 0.0417, *wR*₂ = 0.0976 for all 9393 independent reflections.

Crystal data for **dry_1**: dark-blue single crystals were obtained by heating the crystalline sample of **1** at 105 °C for 4 h in vacuum. Elemental analysis for **dry_1**. C₁₄H₁₀CoN₂O₄S, MW = 361.23. Crystal data for **dry_1**: triclinic, space group *P*-1, *a* = 10.9448(17) Å, *b* = 11.0450(14) Å, *c* = 17.935(4) Å; α = 99.331(14)°, β = 96.762(15)°, γ = 90.269(11)°; *V* = 2123.9(6) Å³; *Z* = 2; *D*_c = 1.695 g·cm⁻³; *F*(000) = 1098; μ = 1.379 mm⁻¹; *R*₁ = 0.2028, *wR*₂ = 0.4767 for 3075 independent reflections with *I* > 2σ(*I*); *R*₁ = 0.3281, *wR*₂ = 0.5315 for all 9328 independent reflections.



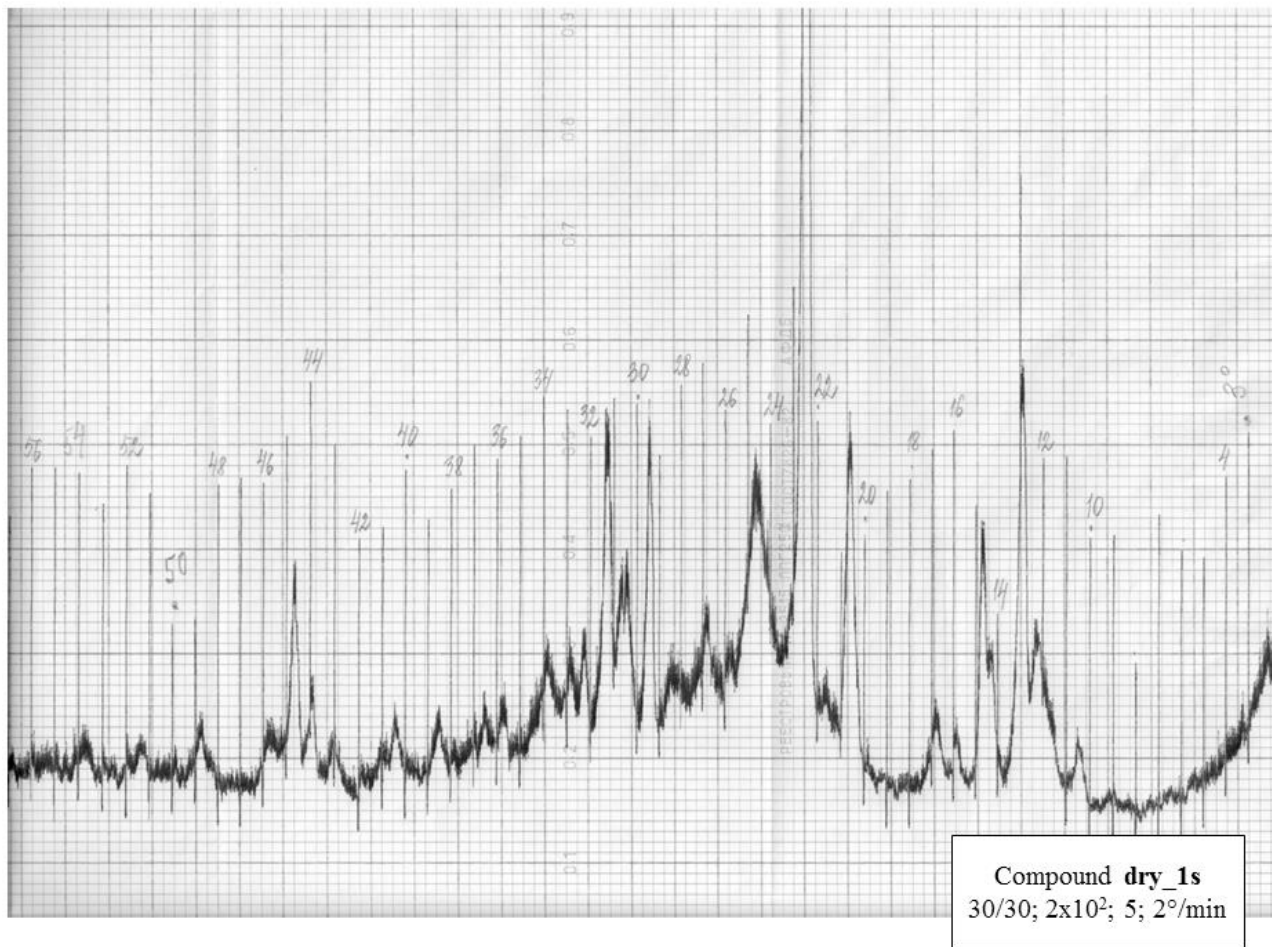


Fig. 1S. Powder diffraction patterns for compounds **1**, **dry_1** and **dry_1s**. The data were obtained on a DRON-UM diffractometer using $\text{FeK}\alpha(\text{av})$ radiation

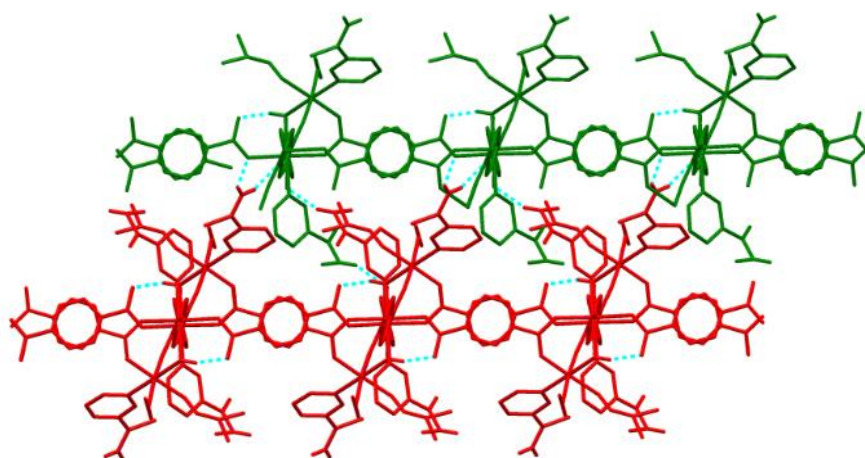


Fig. 2S. Schematic presentation of the interlayer NH...O hydrogen bonds in **1**.

Table 1S. Hydrogen bonds for **1** at 100 K [\AA and $^\circ$].

| D-H...A | d(D-H) | d(H...A) | d(D...A) | $\angle(\text{DHA})$ |
|------------------------|----------|----------|-----------|----------------------|
| N(4)-H(1N4)...O(8)#1 | 0.92 (3) | 2.09(3) | 2.976(3) | 161(2) |
| N(4)-H(2N4)...O(6)#1 | 0.87(3) | 2.10(3) | 2.878(3) | 149(3) |
| N(2)-H(1N2)...O(5)#2 | 0.87(3) | 2.30(3) | 2.966(3) | 133(2) |
| N(2)-H(2N2)...O(7)#2 | 0.77(3) | 2.19(3) | 2.878(3) | 149(3) |
| O(1W)-H(1W1)...O(6) | 0.79 (4) | 1.83(4) | 2.608(2) | 167(3) |
| O(1W)-H(2W1)...O(8) | 0.85 (3) | 1.74(3) | 2.574(2) | 169(3) |
| O(2W)-H(1W2)...O(1D) | 0.89(5) | 1.83(5) | 2.606(10) | 145(5) |
| O(2W)-H(1W2)...O(1C) | 0.89(5) | 1.85(5) | 2.709(4) | 161(5) |
| O(2W)-H(2W2)...O(3W) | 0.84(4) | 1.83(4) | 2.646(3) | 164(3) |
| O(3W)-H(1W3)...O(6) | 0.86(1) | 1.92(2) | 2.747(2) | 162(5) |
| O(3W)-H(2W3)...O(2W)#3 | 0.86(1) | 2.00(1) | 2.859(3) | 172(5) |

Symmetry transformations used to generate equivalent atoms: #1 $x+1, y, z$; #2 $x, y-1, z$; #3 $1-x, 1-y, 1-z$

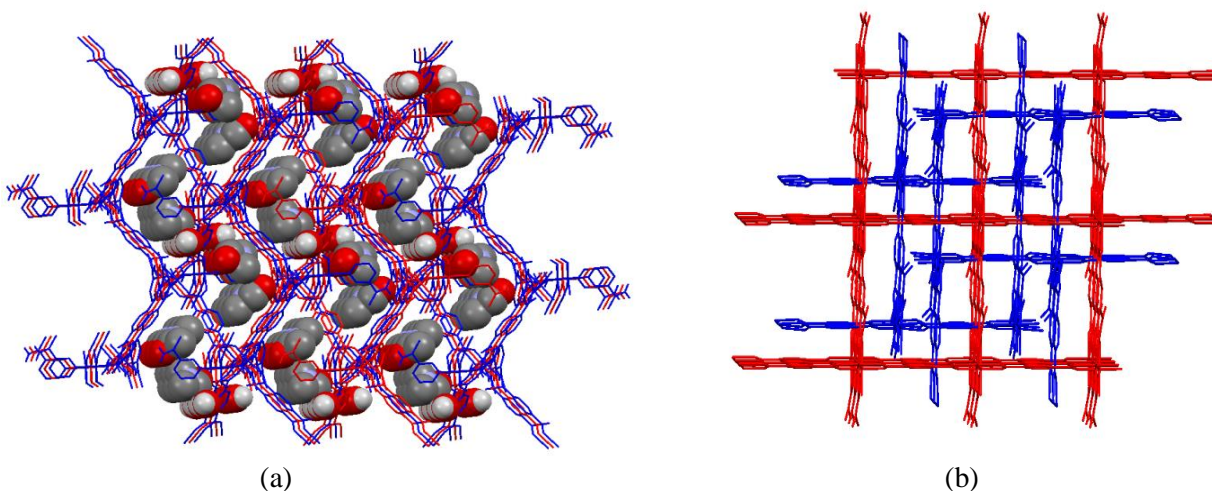


Fig. 3S. Fragments of crystal packing in **1** (a) and **dry_1** (b). Outer sphere solvent molecules in **1** are shown in space-filling mode. C,N-bound H atoms are omitted. Crystallographically identical layers are shown in the same colour.

COMPUTATIONS

Periodical Optimization

The periodical structures were optimised with MOPAC2012 computer program⁴ at PM7 semiempirical theory level.⁵ PM7 Hamiltonian contains empirical dispersion correction which is important for molecular crystals.⁶ The initial atomic coordinates for the crystals **1** and **dry_1** were taken from experiment, with the symmetry reduced to the P1 space group. The electronic structure was assumed to have four unpaired electrons per unit cell, describing four low spin Co(II) ions. In order to predict the unknown structure of crystal **dry_1s**, we modified the crystal structure **1** by substituting each DMF molecule with three methanol molecules and each water molecule with one methanol. The structure was optimised, and the resulting lattice parameters are shown in Table 2S. The structures with other methanol content (6, 10, 12, and 14 molecules per unit cell) were also considered by deleting methanol molecules from the unit cell. The lattice parameters of **dry_1s** are also reported in Table 2S. All versions with 10-18 methanol molecules were found in fair agreements with experiment. The optimised lattice parameters for crystals **1** and **dry_1** are also reported in Table 2S for validation purposes.

Table 2S. PM7 optimized vs experimental lattice parameters for crystals **1**, **dry_1** and **dry_1s**.

| | a | b | c | α | β | γ |
|---|--------------|--------------|--------------|----------------------------|---------------------------|----------------------------|
| Crystal 1 , experimental | 10.61 | 13.43 | 17.84 | 78.86 | 76.42 | 72.3 |
| Crystal 1 , optimized | 10.76 | 13.53 | 17.96 | 73.41 | 75.17 | 74.42 |
| Crystal dry_1s , experimental | 11.11 | 15.73 | 18.08 | 73.81 | 86.67 | 76.43 |
| Crystal dry_1s , optimized with 6MeOH | 12.64 | 14.10 | 18.23 | 73.78 | 70.01 | 53.56 |
| Crystal dry_1s , optimized with 10MeOH | 10.85 | 13.88 | 20.17 | 77.25 | 62.39 | 55.53 |
| Crystal dry_1s , optimized with 12MeOH | 10.78 | 13.49 | 17.90 | 77.92 | 75.44 | 69.53 |
| Crystal dry_1s , optimized with 14MeOH | 10.76 | 13.65 | 18.41 | 75.14 | 73.38 | 67.28 |
| Crystal dry_1s , optimized with 18MeOH | 11.87 | 15.82 | 18.46 | 73.22 | 71.73 | 60.29 |
| Crystal dry_1 , experimental | 10.95 | 11.04 | 17.92 | 99.33 | 96.76 | 90.26 |
| Crystal dry_1 , optimized | 10.51 | 10.62 | 17.51 | 95.64 | 92.87 | 89.91 |

Spectral Predictions

All TDDFT calculations were performed using the Gaussian 2009 suite of programs.⁷ Density Functional Theory with M05-QX exchange-correlation functional⁸ and full-electron 6-31G basis set were used.⁹ In order to avoid the artifactual negative excitations energies, the KS orbitals were reoptimised after stability analysis (keyword **Stable=Opt**) to obtain the most stable ground states. The prediction of the absorption spectra was performed using TD-DFT,¹⁰ from these ground states.

TD-DFT calculations were performed on binuclear complexes taken from the crystal structure of **1** and **dry_1** (protonated to make them neutral), therefore these complexes will be referred as **1c** and **dry_1c**. As shown in Figure 4, **1c** has an absorption peak in 450-500 nm range, and **dry_1c** contains three significant peaks located near 480, 656, and 746 nm. The leading electronic configurations for the strongest absorbing states in 400-800 nm range for **1c** and **dry_1c** are summarized in Table 3S. The absorption band in **1c** is due to a MLCT state, originating from transition between α HOMO (localised on the metal) and α LUMO+2 orbital (localised on the conjugated system in the bdc²⁻) as shown in Fig. 3S.

Table 3S. Electronic structure of the selected excited states in binuclear complexes from structures **1** and **dry_1**. Leading electronic configurations for the absorbing states of **1c** and **dry_1c**.

| Complex | Excited State | Leading configuration | Amplitude | Wavelength | Oscillator strength |
|---------------|---------------|---|-----------|------------|---------------------|
| 1c | 31 | $\alpha\text{HOMO} \rightarrow \alpha\text{LUMO}+2$ | 0.79 | 420nm | 0.0384 |
| dry_1c | 40 | $\alpha\text{HOMO} \rightarrow \alpha\text{LUMO}+7$ | 0.87 | 480nm | 0.0049 |
| dry_1c | 30 | $\beta\text{HOMO}-4 \rightarrow \beta\text{LUMO}$ | 0.84 | 656nm | 0.0022 |

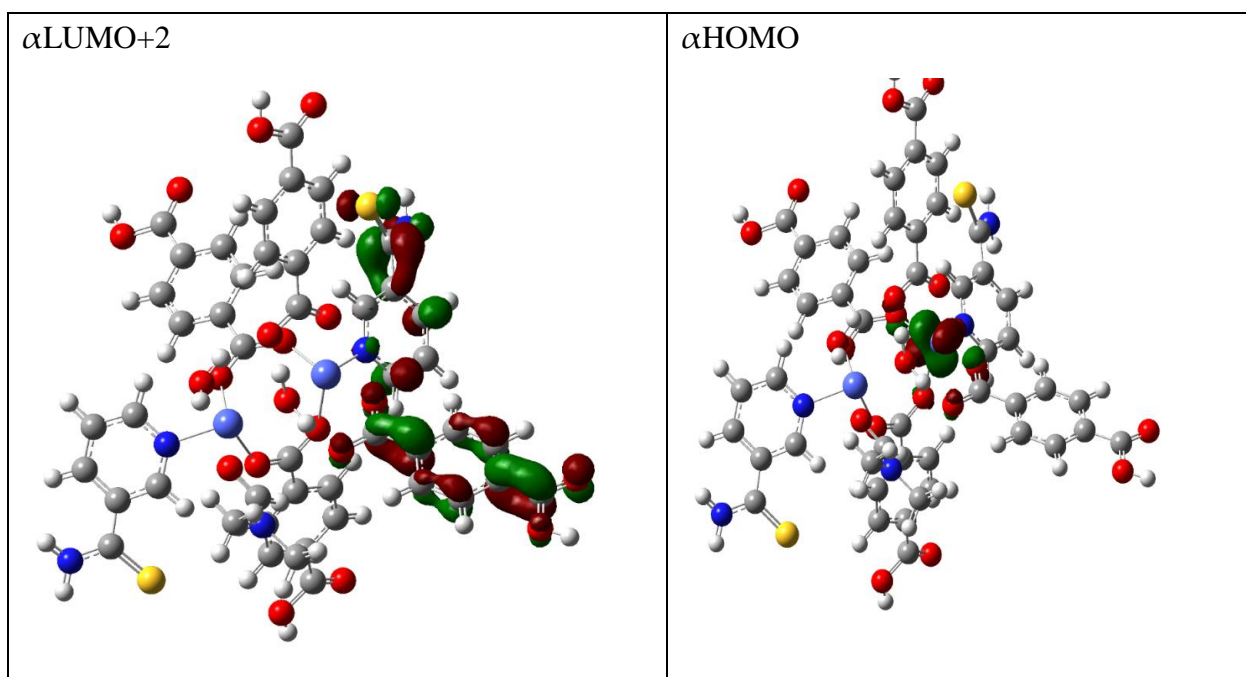


Fig. 4S. Essential Kohn–Sham orbitals in dinuclear complex from **1c**.

Co(II) complexes are known to change colour. For instance, the colour transition for aqueous solutions of CoCl_2 upon rising concentration of chloride ions was interpreted as shift in equilibrium between pink $[\text{CoCl}(\text{H}_2\text{O})_5]^{+1}$ and blue $[\text{CoCl}_2(\text{H}_2\text{O})_2]$ complexes.^{11,12} The respective absorption spectra are shown in Figure 4S, (c). In order to analyse the nature of the colour change upon transition from **1** to **dry_1**, the Time-Dependent Density Functional Theory (TDDFT) was used. All TDDFT calculations were done using the Gaussian 2009 suite of programs,⁷ M05-QX exchange-correlation functional¹³ and all-electron basis set 6-31G.¹⁴

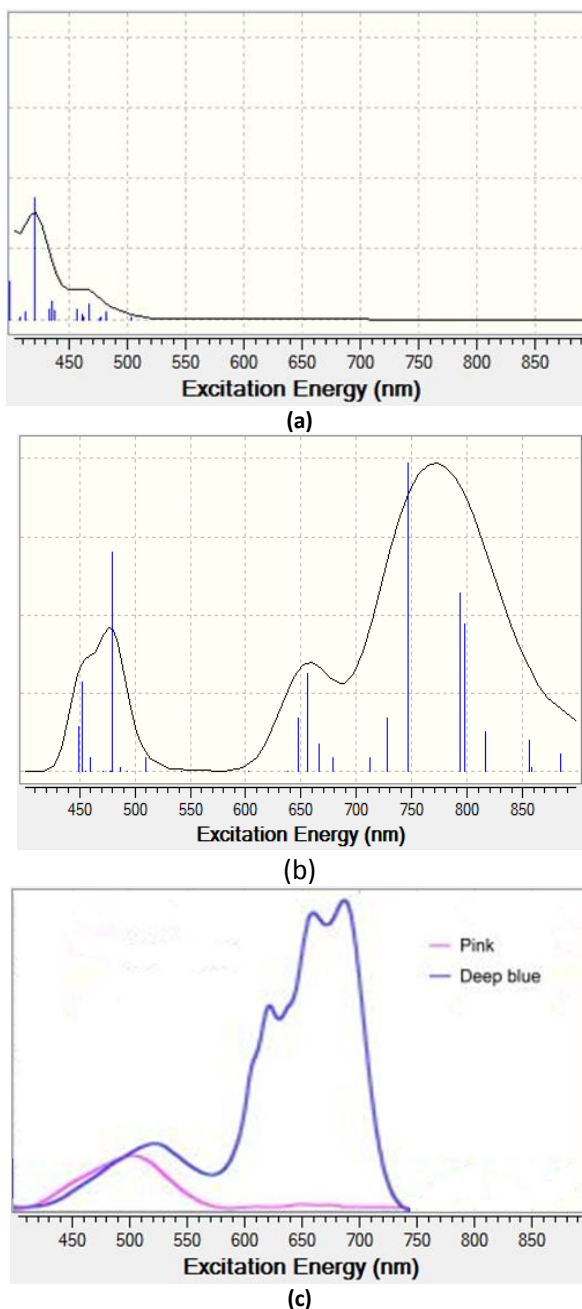


Fig. 5S. TDDFT predicted electronic spectra of: (a) binuclear complex from **1**, and (b) binuclear complex **dry_1**; (c) experimental absorption spectra for pink $[\text{CoCl}(\text{H}_2\text{O})_5]^{+1}$ and blue $[\text{CoCl}_2(\text{H}_2\text{O})_2]$ complexes in aqueous solution (from Ref. [11b]) are also shown.

The binuclear complex **dry_1c** absorbs at three wavelengths. The essential Kohn-Sham orbitals are shown in Figure 5S. The absorption peak near 480 nm is due to LMCT state, corresponding to transition between αHOMO orbital (localized on S-nic ligand) into $\alpha\text{LUMO}+7$, mostly d -orbital on Co(II). The peak close to 656 nm consists of two leading configurations. The latter are composed of MLCT transitions originating from the $\beta\text{HOMO}-4$ and $\beta\text{HOMO}-5$ on Co(II) into the βLUMO orbital on S-nia. The **dry_1** has another MLCT state, which has lower excitation energy due to destabilization of d -orbital of Co metal by the surrounding ligands. The distances from the Co(II) to the bdc^{2-} and S-nia ligands are taken from X-Ray data. The average distances for the Co(II) to oxygen in bdc^{2-} for **1c** is 2.26 Å and for **dry_1c** is 2.02 Å. The average distances for the Co(II) to nitrogen are nearly constant: 2.09 Å for **1c** and 2.05 Å for **dry_1c**.

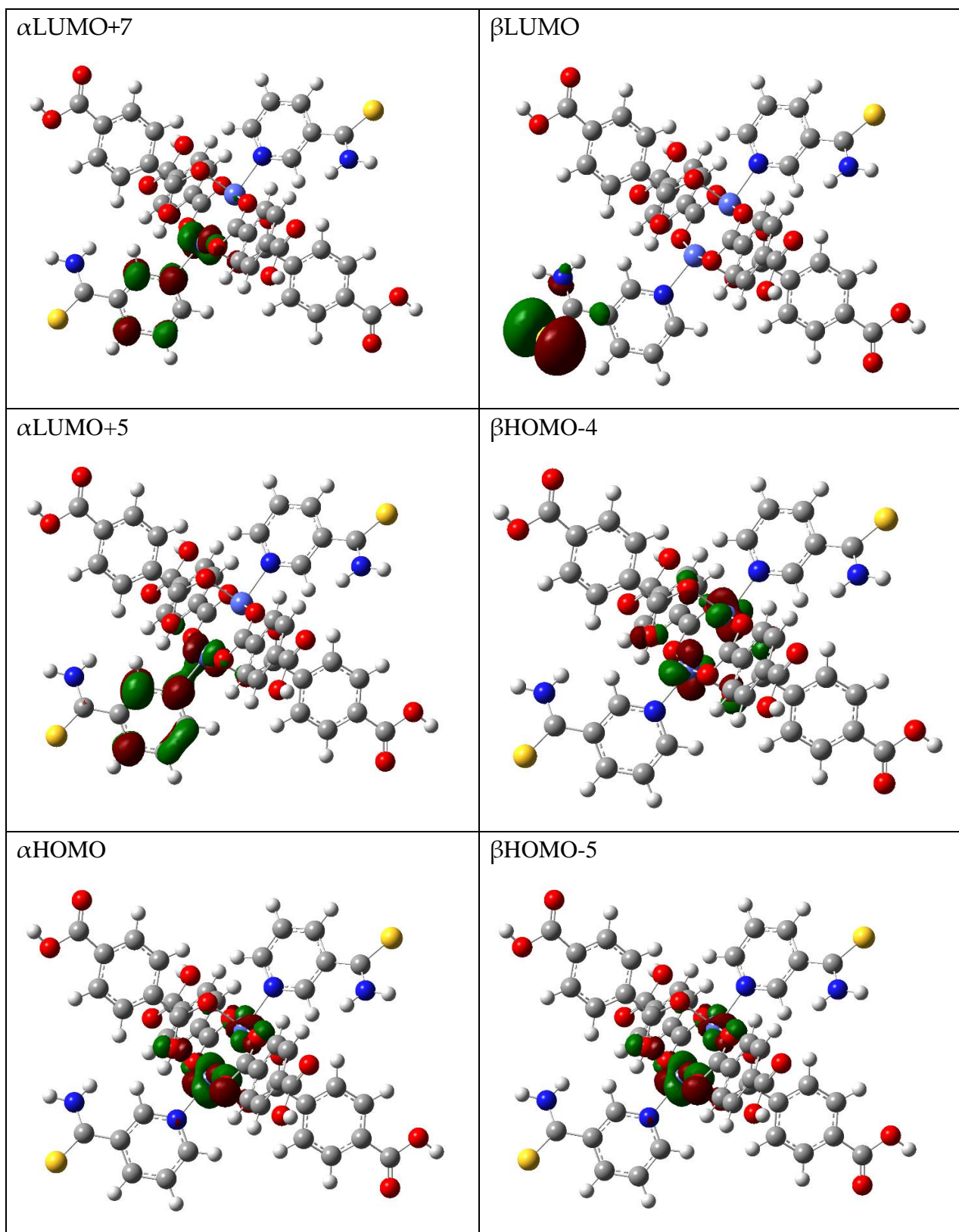


Fig. 6S. Essential Kohn–Sham orbitals in binuclear complex from **dry_1c**.

Thermogravimetric analysis for **1**.

The limits of thermal stability for **1** were proved by thermogravimetric analysis (Fig. 6S). The decomposition occurs in several consecutive stages that in accordance with the literature^{15,16} most probably include: desolvation, release of the neutral S-nia ligand and degradation of the metal-carboxylic skeleton. The first weight loss up to 70 °C corresponds to the loss of one solvated water molecule (found 1.80%; calcd. 1.81%). Up to 177 °C occurs the loss of all remaining solvent molecules, including coordinated and crystallization molecules of dmf as well as eliminating two water molecules inclusive μ_2 -OH₂ bridge. The process is accompanied by the structure reconstruction keeping the coordination skeleton stable. The weight loss is 25.2% (calculated 25.9%). Immediately afterwards occurs the loss of the S-nia molecule in the temperature range 177-232 °C; the process is exothermic, possibly because of reconstructing of **1**. In the 272-314 and 350-383 °C temperature ranges two consecutive decarboxylation processes occur with the mass losses of 4.2% (calculated 4.42%) in both cases. Starting with 385 °C, oxidative degradation takes place leading to the formation of highly exothermic CoO, 14% experimental (calculated 15.08%), which is oxidized in air atmosphere to Co₃O₄. It is decomposed in the range of 934-976 °C with the formation of CoO as a final product.

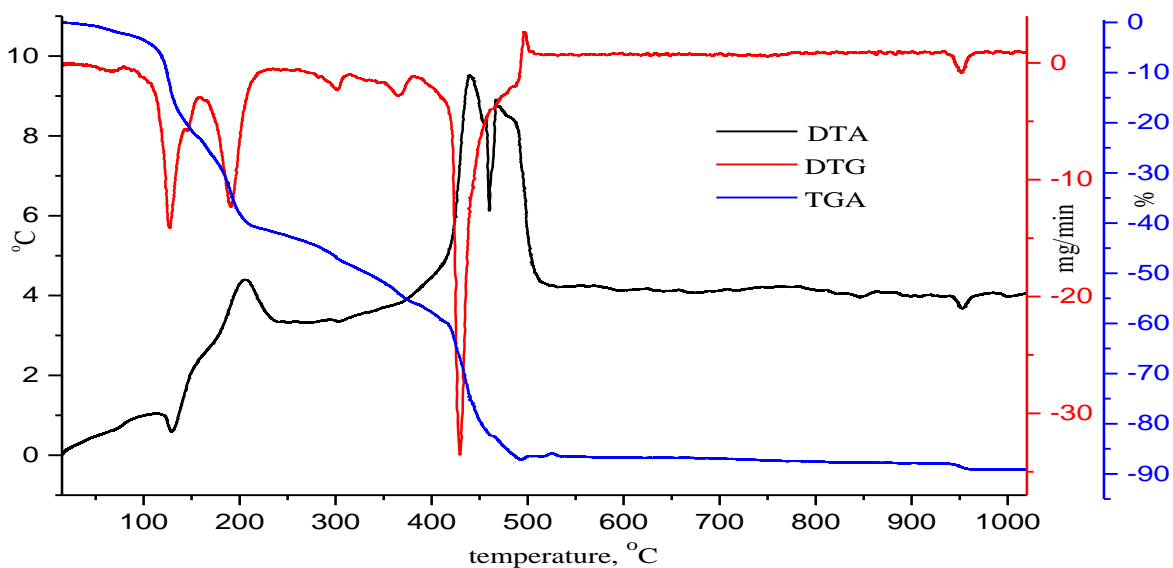


Fig. 7S. TG, DTG and DTA curves for **1** in air atmosphere.

REFERENCES

1. Sheldrick, G.M. Crystal structure refinement with SHELXL, *Acta Crystallogr., Sect. C* . **2015**, C71, 3-8.
2. Edgington, P. R.; McCabe, P.; Macrae, C. F.; Pidcock, E.; Shields, G. P.; Taylor, R.; Towler, M.; Van De Streek, J., Mercury: Visualization and Analysis of Crystal Structures. *J. Appl. Crystallogr.* **2006**, 39, 453-457.
3. Spek, A. L., Structure Validation in Chemical Crystallography. *Acta Crystallogr.* **2009**, D65, 148–1554.
4. Stewart, J. J. P., Mopac2012, Stewart Computational Chemistry Version 14.0831. **2012**.
5. Stewart, J. J. P., Optimization of Parameters for Semiempirical Methods Vi: More Modifications to the NDDO Approximations and Re-Optimization of Parameters. *J. Mol. Model.* **2013**, 19, 1-32.
6. Cardenas-Jiron, G. I.; Masunov, A.; Dannenberg, J. J., Molecular Orbital Study of Crystalline P-Benzoquinone. *J. Phys. Chem. A* **1999**, 103, 7042-7046.
7. Frisch, M. J., et al. *Gaussian 09, Revision D.01*, Gaussian, Inc.: Wallingford CT, 2009.
8. Mikhailov, I. A.; Bondar, M. V.; Belfield, K. D.; Masunov, A. E., Electronic Properties of a New Two-Photon Absorbing Fluorene Derivative: The Role of Hartree-Fock Exchange in the Density Functional Theory Design of Improved Nonlinear Chromophores. *J. Phys. Chem. C* **2009**, 113, 20719-20724.
9. Mitin, A. V.; Baker, J.; Pulay, P., An Improved 6-31g(*) Basis Set for First-Row Transition Metals. *J. Chem. Phys.*, **2003**, 118, 7775-7782.
10. Casida, M. E.; Huix-Rotllant, M., Progress in Time-Dependent Density-Functional Theory. *Ann. Rev. Phys. Chem.*, **2012**, 63, 287-323.
11. (a) A. H. Zeltmann, N.A. Matwiyof and L. O. Morgan, Nuclear magnetic resonance of oxygen-17 and chlorine-35 in aqueous hydrochloric acid solutions of cobalt(II). I. Line shifts and relative abundances of solution species, *J. Phys. Chem.* 1968, **72**, 121; (b) M. Vranes, S. B. Gadzuric, I. J. Zsigrai and S. Dozic, Absorption spectra of cobalt(II) chloride and nitrate complexes in aqueous calcium nitrate–ammonium nitrate melts: The influence of solvent composition, *J. Mol. Liq.*, 2010, **152**, 34.
12. N. K. T. Koga, M. Sakamoto and Y. Furukawa, *Chem. Educator*, 2009, **14**, 225.
13. I. A. Mikhailov, M. V. Bondar, K. D. Belfield and A. E. Masunov, Electronic Properties of a New Two-Photon Absorbing Fluorene Derivative: The Role of Hartree–Fock Exchange in the Density Functional Theory Design of Improved Nonlinear Chromophore, *J. Phys. Chem. C*, 2009, **113**, 20719–20724.
14. (a) W. J. Hehre, R. Ditchfield and J. A. Pople, Self—Consistent Molecular Orbital Methods. XII. Further Extensions of Gaussian—Type Basis Sets for Use in Molecular Orbital Studies of Organic Molecules *J. Chem. Phys.*, 1972, **56**, 2257; (b) V. A. Rassolov, J. A. Pople, M. A. Ratner and T. L. Windus, 6-31G* basis set for atoms K through Zn *J. Chem. Phys.*, 1998, **109**, 1223–1229.
15. Köse, D.; Ay, A.; Şahin, O.; Büyükgüngör, O., A Mononuclear, Mixed (Salicylato) (Nicotinamide) Complex of Zn(II) with Penta- and Hexa-Coordination Sites: A Novel Framework Structure. *J. Iran Chem. Soc.* **2012**, 9, 591-597.
16. Köse, D. A.; Gökçe, G.; Gökçe, S.; Uzun, İ. P-Chlorobenzoate Complexes of Ni(II), Zn(II) and Cd(II). *J. Therm. Anal. Calorim.* **2009**, 95, 247-251.